Extension of the Bimodal Intraseasonal Oscillation Index using JRA-55 reanalysis

Kazuyoshi KIKUCHI

International Pacific Research center, School of Ocean and Earth Science and Technology, University of Hawaii at Manoa Honolulu HI 96822

Submitted to Clim. Dyn.

August 2019 (revision)

School of Ocean and Earth Science and Technology Contribution Number XXXX and International Pacific Research Center Contribution Number YYY.

Corresponding author:
Kazuyoshi Kikuchi
International Pacific Research Center, University of Hawaii
1680 East West Road, POST Bldg. 401, Honolulu, HI 96822, USA
E-mail: kazuyosh@hawaii.edu
Tel: +808-956-5019, Fax: +808-956-9425
ORCID: 0000-0002-6200-0968

Abstract

This study aims to extend the bimodal intraseasonal oscillation (ISO) index, developed by Kikuchi et al., 2012, using JRA-55 reanalysis back in time to 1958. The bimodal ISO index is composed of two distinct ISO indices: the Madden-Julian oscillation (MJO) index and the boreal summer ISO (BSISO) index, each aiming to capture the ISO behavior during boreal winter and summer, respectively. These indices are derived by means of extended empirical orthogonal function (EEOF) analysis applied to outgoing longwave radiation (OLR) during boreal winter and summer, respectively. By combining the MJO and BSISO indices, the state of the ISO can be reasonably represented over the course of the year. First, the original index is updated using observed OLR until recently (-Jan. 2017) with a modification of the use of extended winter and summer months (Dec.-Apr./Jun.-Oct.) instead of normal winter and summer months (Dec.-Feb./Jun.-Aug) in EEOF analysis. The updated version is quite consistent with the original counterpart, whereas it is arguably able to represent the ISO more faithfully throughout the year. In the same manner, a JRA-55-based index is constructed. Although JRA-55 OLR has systematic biases, the resulting JRA-55-based bimodal ISO index is in excellent agreement with the observation-based index. A comparison between JRA-55 and its subset, JRA-55C (satellite observations are not assimilated at all) suggests that the JRA-55-based index is reliable even in the pre-satellite era. Interannual variability and long-term trend of the ISO activity are also discussed. The newly developed, long-term JRA-55-based index will be useful for a number of applications.

Keywords: ISO, MJO, BSISO, JRA-55, index

1. Introduction

The tropical intraseasonal oscillation (ISO), characterized by the periodicity of 30-60 (90) day, is the predominant phenomenon in the tropics throughout the year (Madden and Julian 1994; Lau and Waliser 2012) and has a profound influence on a wide range of space-time scale phenomena (e.g., Zhang 2013; Serra et al. 2014). Here we use the term "ISO" to refer to the 30-60 day oscillation in a broad sense that includes, but is not identical to, the so-called Madden-Julian oscillation (MJO) (Madden and Julian 1971, 1972), which is often regarded as representing the ISO during boreal winter. As discussed below, the 30-60 day oscillation during boreal summer displays distinct spatio-temporal behavior (e.g., Yasunari 1979; Knutson and Weickmann 1987; Wang and Rui 1990) and is variously referred to as the boreal summer MJO, boreal summer ISO (BSISO), and monsoon ISO (MISO) (we prefer to use the term "BSISO"). Thus, we prefer to view the ISO as comprising of the MJO and the BSISO. Despite its importance, how to define the ISO is diverse. People used different approaches to define the ISO (a review can be found in Kikuchi et al. 2012), particularly before the seminal study of Wheeler and Hendon (2004). They developed an index, referred to as an all-season real-time multivariate MJO (RMM) index, by isolating common features of the ISO that exist throughout the year by applying empirical orthogonal function (EOF) analysis to combined fields of near-equatorially averaged 850-hPa zonal wind, 200-hPa zonal wind, and outgoing longwave radiation (OLR). Quite a large number of studies have benefitted from the index to address different aspects of the ISO and associated variability (e.g., Cassou 2008; Kim et al. 2009; Wheeler et al. 2009; Kim et al. 2018).

Although it is a remarkable approach, the degree to which the RMM index is able to faithfully represent the ISO throughout the year is in question. It has long been recognized that the ISO during boreal winter is characterized by pronounced slow eastward propagation along the equator over the Indo-Pacific warm pool region (e.g., Lau and Chan 1985; Knutson and Weickmann 1987), while that during boreal summer by northward/northwestward migration of convection over the northern Indian Ocean and western North Pacific as well as slow eastward propagation along the equator (e.g., Lau and Chan 1986; Wang and Rui 1990). In addition, recent studies have pointed out that the RMM index is representative rather of the dynamical fields than of OLR (Straub 2013; Ventrice et al. 2013; Liu et al. 2016), suggesting that it is inadequate for capturing the ISO convection. Recently, some efforts have been made to construct a new OLR-based ISO index taking the ISO seasonal cycle into account. Kikuchi et al. (2012) proposed a bimodal ISO index, on the basis of extended EOF (EEOF) analysis, that consists of the so-called MJO mode and BSISO mode, which represents the typical spatio-temporal behaviors of the ISO during boreal winter and summer, respectively. Kiladis et al. (2014) developed another index, referred to as an OLR-MJO index (OMI), that relies on daily-varying EOFs derived from windowed data centered on the target day. These newly developed ISO indices arguably much better represent individual ISO events than the RMM index throughout the year (Kikuchi et al. 2012; Wang et al. 2018b). This study particularly concerns the bimodal ISO index.

So far the bimodal ISO index has been used to address a variety of topics including assessment of models' ability to reproduce the ISO (Kikuchi et al. 2017; Shibuya et al. 2018; Nakano and Kikuchi 2019), description of ISO-tropical cyclone relationship (Hirata and Kawamura 2014; Yoshida et al. 2014), and examination of decadal change in the BSISO (Yamaura and Kajikawa 2017) and of air-sea fluxes associated with the BSISO (Konda and Vissa 2019). Nonetheless, the index may not be able to provide sufficient opportunities to address certain aspects of the ISO and associated variability on timescales ranging from interannual to multidecadal, because the satellite-derived OLR data (Liebmann and Smith 1996) on which the index relies is only available from mid-1970s at best.

In the last decade or so, efforts have been devoted, using up-to-date data assimilation (DA) systems, to construct comprehensive reanalysis that covers the period from late 1950s (Uppala et al. 2005; Kobayashi et al. 2015). Of particular note is the most recently developed reanalysis by the Japan Meteorological Agency (JMA), the second Japanese global atmospheric reanalysis (JRA-55) (Kobayashi et al. 2015). Since its predecessor, JRA-25 (Onogi et al. 2007), JMA's operational NWP system has improved in many respects, including revision of the longwave radiation scheme, introduction of four-dimensional variational analysis and variational bias correction for satellite radiances. These improvements have led to significant reduction in model biases, improved consistency of the dynamical fields, and advanced handling of satellite radiances (Kobayashi et al. 2015). It has been reported that JRA-55, compared to other reanalysis, is able to well reproduce various tropical subseasonal variability including the ISO and convectively coupled equatorial waves (CCEWs) (Harada et al. 2016). Another advantage of JRA-55 is that it provides JRA-55 Conventional (JRA-55C) as its subset, which uses only conventional observations based on the same DA system and the same boundary conditions as JRA-55, which provides us with an opportunity to examine the degree to which reanalysis in the pre-satellite era is reliable.

The purpose of this study is to extend the bimodal ISO index by using JRA-55 reanalysis back in time to 1958. First of all, we update the bimodal ISO index using observational data until recently with a slight modification in which the way two ISO modes are defined. It is found that this modification improves the representation of the ISO over the course of the year, though most of the results that have been obtained using the original index would be insensitive to this modification. Then, in the same manner, a JRA-55-based bimodal ISO index is constructed. The newly developed, JRA-55-based ISO index will provide good opportunities to better understand the variability of the ISO and associated variability on longer timescales. This study paves the way for a number of possible future ramifications.

The paper is constructed as follows. Section 2 describes the data and methodology to be used. In Section 3, we update the bimodal ISO index using most up-to-date OLR data with the minor modification. In Section 4 we construct the bimodal ISO index using JRA-55 and discuss its reliability and argue some aspects. Section 5 concludes this paper.

2. Data and methodology

2.1. Data

Satellite- and reanalysis-derived OLR datasets are primarily used in this study. Daily NOAA interpolated OLR dataset at a horizontal resolution of 2.5º latitude/longitude (Liebmann and Smith 1996) is available, at the time of writing, for the period of June 1974 to January 2017, with the gap between 17 March and 31 December 1978. In favor of not including the data gap period, we use the dataset for the period 1979 to January 2017. JRA-55 (Kobayashi et al. 2015) and its subset, JRA-55C (Kobayashi et al. 2014) are also used in this study. OLR at the nominal top of the atmosphere is provided as a forecast variable every three hours as an average from the beginning of forecasts up to 3 hours. JRA-55 is available from 1958 to present and we used it for the period 1958-2017. JRA-55C, in contrast, covers the period from November 1972, when JRA-55 starts to use satellite data, to 2012. JRA-55C assimilates only conventional observations that exist throughout the entire period covered by JRA-55, including land and marine surface data, upper air data, and tropical cyclone wind retrievals. Thus, by comparing JRA-55 and JRA-55C we can assess the impact of the use of satellite observations into data assimilation. Both reanalysis datasets are provided at a horizontal resolution of either 1.25º latitude/longitude or model grid (TL319~55 km). We constructed and used coarse-grained data of reanalysis with 2.5º latitude/longitude, which is in line with the NOAA OLR dataset.

2.2. Construction of the bimodal ISO index

We briefly review how the bimodal ISO index is constructed. Please see Kikuchi et al. (2012) for a comprehensive description. First, the intraseasonal component is isolated by applying 25-90 day Lanczos bandpass filter (Duchon 1979) to OLR data. Extended EOF analysis (Weare and Nasstrom 1982) with three time lags (−10, −5, and 0 days) is employed to extract the typical spatio-temporal behavior of the ISO convection during boreal winter and summer, respectively. In Kikuchi et al. (2012), the winter and summer months are defined as December-February (DJF) and June-August (JJA), respectively. This choice, however, is modified in this study (the winter as December-April, while the summer June-October), as discussed more in detail in the next section. The first two EEOFs for each season are used to define the MJO mode and the BSISO mode. Finally, the corresponding principal components (PCs) for the entire period are obtained by projecting the extended intraseasonal OLR anomaly fields composed of the same three time lags onto each EEOF for each mode, giving rise to the MJO index and the BSISO index, respectively. At any given time, the state of the ISO is classified into significant MJO, significant BSISO, or insignificant ISO based on the normalized amplitude ($A^* = (PC_1^{*2} + PC_2^{*2})^{1/2}$) and non-normalized amplitude $A = (PC_1^2 + PC_2^2)^{1/2}$ of the MJO and BSISO indices, where PC^* represents the normalized PC by one standard deviation during the period the EEOF analysis was performed, as schematically summarized in Fig. 1 (see Kikuchi et

Fig. 1

al. 2012 for a more detailed discussion)

3. Update of the bimodal ISO index

We update the bimodal ISO index using satellite-derived data until recently with the modification in the definition of the MJO mode and the BSISO mode. In the intention of isolating typical spatio-temporal behavior of the ISO that is pronounced during two extreme seasons, Kikuchi et al. (2012) applies EEOF analysis to data during DJF and JJA. It was found that the MJO mode is able to represent the ISO behavior well from December to April (DJFMA), while the BSISO from June to October (JJASO), and May and November are transitional months. This bimodality nature of the ISO was corroborated by later studies based on different approaches (Kiladis et al. 2014; Szekely et al. 2016). In light of this bimodality nature, it may be more reasonable to define the MJO mode and the BSISO mode from data during DJFMA and JJASO, respectively. In other words, the original treatment may have overlooked ISO events that occur outside of DJF and JJA.

Fig. 2

Figure 2 shows the leading two EEOFs for 1979-2009 DJF and JJA, which correspond to the original EEOFs derived by Kikuchi et al. (2012) and those for DJFMA and JJASO using 1979-January 2017 data ("updated version"). The EEOFs are scaled by multiplying by one standard deviation of the corresponding PCs during the period each EEOF analysis is carried out so that the amplitudes reflect the typical magnitude of an event. The updated EEOFs seem to be somewhat smoother and the contributions of each EEOF become somewhat smaller, both of which are due to the use of the extended months rather than of the longer period (not shown), although both versions overall exhibit quite consistent results (Table 1). In the end, the corresponding PCs are remarkably consistent between the original and updated versions (Fig. 3

Fig. 3

Table 1

and Table 1), with a time lag of 1 day suggesting that the spatio-temporal pattern that accounts for the largest variance shifts in a systematic manner in time by 1 day.

Meanwhile, the minor modification improves the representation of the ISO throughout the year. Figure 4 shows the climatological annual cycle of the MJO mode and the BSISO mode Fig. 4 in terms of their non-normalized amplitudes. It is evident that the predominant ISO mode switches in May and November, which is consistent with other studies (Kiladis et al. 2014; Szekely et al. 2016). A notable feature is that the amplitude of each ISO mode in the updated version, relative to the original version, become larger outside of its typical target season (DJF or JJA), whereas it almost remains the same in its target season. Another interesting feature is large drops in the BSISO amplitude in September in both versions, which will not be examined in detail in this study, though. As a result of the minor modification, significant ISO days are picked out more uniformly across months in the updated version (Fig. 5). In particular, large Fig. 5 increases in April, May, October, and November are obvious features (which are also expected from Fig. 4 and can be seen in Fig. 3). In the end, the average frequency of occurrence increases from 0.52 to 0.59, which is in better agreement with other ISO indices such as the RMM (0.62) and OMI (0.57).

From the discussion above, we conclude that the updated bimodal ISO index yields highly consistent results with the original index, while it is able to more faithfully represent the ISO over the course of the year. From now on, we will use the updated version.

4. Extension of the bimodal ISO index using JRA-55

4.1. Climatology and intraseasonal variance

First, we examine how OLR is represented in JRA-55. Fig. 6 shows the climatology of OLR and Fig. 6

intraseasonal (25-90 day) variance of OLR anomalies. As pointed out earlier, the climatological OLR in JRA55 has large positive biases in deep convective areas, due most likely to underestimation of cloud radiative effects (Kobayashi et al. 2015). Also evident in deep convective areas is large negative biases in the intraseasonal variance. It is underestimated by a factor of ~ 2, which is consistent with an earlier report by Harada et al. (2016). Not only the amplitude but also the patterns are different slightly. Locations of minimum climatological OLR are somewhat shifted, including those over the central Africa. The patterns of the intraseasonal variances are, to some extent, consistent, while the large peak over the equatorial central Indian Ocean is not evident in JRA-55. Despite these large biases, it has been reported that subseasonal tropical variability including the ISO and CCEWs, in general, is relatively well reproduced in terms of signal-to-noise ratio compared to other reanalysis datasets (Harada et al. 2016).

4.2. Development of the bimodal ISO index using JRA-55 data

As described in Section 2.2, we construct a bimodal ISO index using JRA-55 OLR data. As in the updated version discussed in the previous section, we use the extended months to isolate the MJO and the BSISO modes. Shown in Fig. 7 are the first two EEOFs for both modes based on 1958-2017 period. Compared to the observation (Fig. 2), there are some differences. The amplitudes of the EEOFs are smaller by a factor of ~2, which is consistent with Fig. 6. The JRA-55-based EEOFs appear to have smaller-scale features (i.e., noisier) and weak tendency over the central Indian Ocean for both seasons, whereas major features are well captured for both modes such as the dipole structure in the Indo-Pacific warm pool region for the MJO and the northwest-southeast tilted convective band for the BSISO. Indeed, the correlations between the observation- and the JRA-55-based EEOFs are relatively high (Table 2). Note that these results are robust regardless of the choice of the period used. For instance, the EEOFs yield quite

Fig. 7

Table 2

similar patterns if using the same period as the observation (i.e., 1979-January 2017, not shown).

It is remarkable that the resulting PCs have exceptionally high correlations with those obtained from the observation (Table 2), although there are slight time lags (1 or 2 days at most) that would not make much difference (i.e., small compared to the ISO periodicity, 30-60 days). In other words, the biases in the representation of the ISO in JRA-55 are so systematic that they are mainly absorbed by EEOFs and have little effect on PCs.

Finally, it is worth noting that constructing a bimodal ISO index by projecting JRA-55 OLR data onto the observed EEOFs is another option. In fact, that approach works as well (not shown). However, in the spirit of developing an independent index, we take the approach mentioned above.

4.3. How reliable is the JRA-55-based ISO index in the pre-satellite era?

We have shown that the JRA-55-based ISO index is highly consistent with the observation-based index. Then, it is natural to ask how reliable is the index in the pre-satellite era? We address that issue by comparing the JRA-55 and its subset JRA-55C (not assimilating satellite observations at all). Before comparing the two indices in detail, we compare snapshots of OLR on a particular day (27 October 2011, Fig. 8) to gain a sense of the degree to which JRA-55 is consistent with or different from JRA-55C. This is a date in the midst of the first ISO event that took place during the CINDY/DYNAMO field campaign (Gottschalck et al. 2013; Yoneyama et al. 2013), which has been rigorously examined in many different respects (e.g., Johnson et al. 2015; Kikuchi et al. 2018). According to the original bimodal ISO index[1], the

Fig. 8

[1] see http://iprc.soest.hawaii.edu/users/kazuyosh/Bimodal_ISO.html

normalized amplitudes of both MJO and BSISO modes are greater than 1 (1.02 and 1.54, respectively), although the non-normalized amplitude of the BSISO mode (530) is much greater than that of the MJO mode (398), indicating that this event can identified as a significant BSISO event (see Fig. 1). In addition, this particular date corresponds to phase 3 of the BSISO. In fact, the convective features over the IO in the observation (Fig. 8a) look very similar to phase 3 of the BSISO composite (Fig. 12). JRA-55 and JRA-55C both appear to capture the major features of this convective signal, although the amplitudes are much smaller, as has been discussed so far. Upon close inspection, there are differences between JRA-55 and JRA-55C, yet they are mainly outside of the major BSISO convection.

Table 3

Figure 9 shows the two leading EEOFs for DJFMA and JJASO obtained using JRA-55C. The patterns are similar to those based on JRA-55 (Fig. 7). The correlations between them, indeed, are very high as well as their PCs (Table 3). Therefore, we conclude that the bimodal ISO index based on JRA-55 OLR is arguably reliable even in the pre-satellite era, to the extent that the conventional observations in the pre-satellite era are dense in space and time and reliable.

4.4. Seasonal cycle and composite structures

Fig. 10

We examine the seasonal cycle and composite structures of the ISO represented in JRA-55. Figure 10 shows the monthly frequency of occurrence of significant ISO days based on the JRA-55 ISO index for the period 1958-2017 (color bars) in conjunction with that for the period 1979-2017 based on the JRA-55 (black line) and on the observation (i.e., Fig. 5b, green line). It is clear that the overall shape of the seasonal cycle is in good agreement between the observation and the JRA-55. On the basis of a comparison for the overlapping period between the observation and the JRA-55 (i.e., black line vs. green line), it is suggested that the JRA-55 tends to overestimate or underestimate the ISO amplitude in some months (e.g., the JRA-55 tends to overestimate the MJO amplitude in Feb, Mar, and Nov, while it tends to underestimate in Apr). The largest discrepancy occurs in May, in which the MJO and BSISO amplitudes are both underestimated in the JRA-55, resulting in a fewer number of total significant ISO days by ~20 %. On the other hand, a comparison in the JRA-55 between the two periods (i.e., color bar and black line) suggests the BSISO amplitude tends to be lower in the pre-satellite era, which will be discussed more in detail in the next subsection in relation to linear trends.

Based on significant ISO events, we construct composites based on the two indices. As in previous studies (e.g., Kikuchi et al. 2012), we separate the ISO into 8 phases. Figures 11 and 12 show the composite structures of OLR anomalies for the MJO and BSISO modes, respectively. Given that the composite structures are insensitive to the choice of the period used, we show the results based on 1958-2017 for JRA-55. Thus, the number of days used to construct the composite is larger for JRA-55 than for the observation. The spatial features in JRA-55 seem to be somewhat noisier or contain finer-scale features, which is of course consistent with the EEOFs (Fig. 7), although the fundamental features of both the MJO and BSISO are in good agreement, albeit the smaller amplitude in JRA-55 by a factor of ~2.

Fig. 11

Fig. 12

In both composites, the MJO starts to appear over the equatorial western Indian Ocean and propagates eastward. When it moves across the Maritime Continent, the convection seems to split into northern and southern branches, the southern branches being stronger. Finally, the convection moves southeastward over the western Pacific and decays. In contrast, the BSISO convection starts to appear over the central Indian Ocean in phase 1 and propagate both eastward and northwestward over the Indian Ocean (in phases 2-3), giving rise to a northwest-southeast tilted convection band in phases 4-6. The northwestward propagating component over the northern Indian Ocean continues to move further northwestward and dissipates over the Indian subcontinent, while the eastward propagating component starts to move northwestward when it arrives over the western Pacific.

4.5. Interannual variability and linear trends

It is beyond the scope of this study to rigorously examine the interannual and long-term variability of the ISO, although it is of interest to look at how the ISO activity varies over the course of the last six decades. Figure 13 shows time series of the ISO amplitude in terms of the MJO and BSISO modes based on the JRA-55-based index. As has been discussed, the MJO mode and the BSISO mode tend to be predominant during boreal winter and summer, respectively. It is evident that both ISO modes undergo significant year-to-year variations in activity. For instance, there were epochs that both ISO activities remained relatively high for a long period of time such as from 2004 to 2010, while they remained low in some epochs such as from 1982 to early 1984 (which is quite consistent with Wheeler and Hendon 2004).

Fig. 13

Then, what controls these year-to-year changes in the ISO activity? Many previous studies have focused on the effect of El Niño and the Southern Oscillation (ENSO). Although the evolution characteristics of the ISO is affected by ENSO (e.g., Pang et al. 2016; Wang et al. 2018a), the overall level of ISO activity tends to be uncorrelated with ENSO (Hendon et al. 1999; Slingo et al. 1999; Hendon et al. 2007). Recently, the novel idea that the stratospheric quasi biennial oscillation (QBO) controls the ISO activity during boreal winter has emerged (Yoo and Son 2016; Son et al. 2017). Using the newly developed JRA-55-based ISO index, we address these issues. Table 4 summarizes the simultaneous relationship of the level of ISO activity with ENSO and the QBO. The results are in good agreement with previous studies. The overall activities of both ISO modes are uncorrelated with ENSO, whereas the activity of the

Table 4

MJO mode correlates with QBO (significant correlations in the upper and lower stratosphere with switching sign) throughout the extended winter. The relatively lower correlations, compared to Son et al. (2017), are primarily due to the use of the longer period used, as will be discussed below.

Detailed year-to-year variations of the ISO activity may be well described by means of the wavelet transform. Figure 14 shows normalized wavelet spectra of the 3 month running mean MJO and BSISO amplitudes calculated following Torrence and Compo (1998). By construction, the annual cycle is most pronounced. Both spectra vary on multiple timescales, although no specific timescale appears to exist that strongly controls both of the ISO modes. There are several interesting features to note. First, both modes do not appear to be associated closely with ENSO, which is characterized by 2-7 years periodicity and was relatively active from 1960s to 1990s (Torrence and Compo 1998). Second, pronounced two-year peaks sometimes appear in both spectra, while they are nonstationary. Perhaps what is worth mentioning is that the two-year peaks in the MJO spectrum appear exclusively in the last three decades, suggesting that the good MJO-QBO relationship has emerged since 1980s (Klotzbach et al. 2019). Third, the spectrum of the BSISO index has more power on longer timescales such as 4-8 years (which seems to be different from ENSO in nature) and multidecadal (15~30 years) (Yamaura and Kajikawa 2017). This is probably why we have not been able to explain the interannual variability of the overall level of BSISO activity, as opposed to the MJO counterpart (like the MJO-QBO relationship).

Fig. 14

In order to gain better insight into what controls the year-to-year variability of BSISO activity, we examine the relationship with sea surface temperature (SST) using the Extended Reconstructed SST (ERSST) (Huang et al. 2017). Variability associated with two distinct timescales, 4-8 years (interannual) and longer than 13 years (interdecadal), are isolated by means of the Fourier transform. Since the available data length is limited (59 years), we use a simple Fourier transform approach instead of the use of a sophisticated digital filter (Emery and Thomson 1997). That is, after removing the linear trend from the yearly time series, we retained the 8-16th and 1-5th components of the Fourier transform for the interannual and interdecadal components, respectively. Figure 15 shows correlations between the BSISO activity and the SST anomalies on the two timescales for JJA (results are similar for JJASO). For the interannual component, it is difficult to find any well-defined structure. For the interdecadal component, on the other hand, there is a pattern that is to some extent reminiscent of the interdecadal Pacific oscillation (IPO), which is characterized by a tripole structure with the nodes over the eastern North Pacific, eastern South Pacific, and equatorial western Pacific (Folland 1999; Power et al. 1999). However, the correlation between the BSISO activity and the IPO index (Henley et al. 2015) is not high (-0.36). Another feature worth noting is that there are significant positive SST anomalies in the northern Indian Ocean around the Indian Peninsula. In summary, the degree to which how these SST anomalies affect the overall level of BSISO activity is still unclear.

Fig. 15

Another intriguing feature inferred from Fig. 13 is that there may be linear trends. Apparently, the overall level of activity of both modes in the last 1.5 decades appear to be much greater than the first 1.5 decades of the period. Similar positive trends in ISO activity were pointed out by Slingo et al. (1999) and Jones and Carvalho (2006), who used the National Centers for Environmental Prediction/National Center for Atmospheric Research (NCEP/NCAR) re-analysis (Kalnay et al. 1996), which suffered from several human processing errors (Kanamitsu et al. 2002), though. We calculate linear trends by means of least-squares, and assess their statistical significance using a Student's-t test taking into account serial autocorrelation based on the method of Santer et al. (2000). Figure 16 shows time series of the MJO and BSISO variance based on the JRA-55 and the observation in conjunction with their linear trends. It is evident that the time series are highly coherent between the JRA-55 and observation on the interannual timescale (the correlations are over 0.95). However, the estimated linear trends are significantly different. The trends in the MJO variance (Fig. 16a) based on the JRA-55 are significantly upward (0.13 decade^{-1} corresponding to ~9 % decade^{-1}) for both DJF and DJFMA, whereas that based on the observation are either slightly upward, 0.034 decade^{-1} (~2 % decade^{-1}) for DJF or downward -0.031 decade^{-1} (~-2 % decade^{-1}) for DJFMA. The trends in the BSISO variance (Fig. 16b), in contrast, are consistently upward both in the JRA-55 and the observation, yet their magnitudes are much smaller in the observation: they are in the rage of 0.039-0.11 decade^{-1} (~2-6 % decade^{-1}) in the observation as opposed to 0.15-0.22 decade^{-1} (~10-16 % decade^{-1}) in the JRA-55. Note that the linear trends in the JRA-55 are similarly positive and much larger than in the observation for the same period as the observation (not shown). Recently, Oliver (2016) estimated the linear trend in ISO activity by constructing a bivariate index using surface pressure at a finite number of locations from the Twentieth-Century Reanalysis (20CR; Compo et al. 2011). He showed that the trend in ISO amplitude varies from nearly zero to an increase of ~30% over the 20th century (i.e., ~7% decade^{-1} in variance) depending on the locations used and suggested that we need to be aware of the observational measurements. At this moment, it is difficult to draw a robust conclusion on the linear trend in ISO activity, yet it may be reasonable to say that the JRA-55 for some reason tends to exaggerate or overestimate the amplitude of the ISO in recent decades, as is inferred from Fig. 16.

Fig. 16

5. Conclusions

We updated and extended the bimodal ISO index introduced by Kikuchi et al. (2012) using OLR from both satellite observations and JRA-55. To better represent the ISO over the course of the year, we made a slight modification in defining the MJO mode and the BSISO mode. Originally, the MJO and BSISO modes rely on the first two EEOFs derived from the normal winter (DJF) and summer (JJA) months, respectively. This setting, however, results in overlooking ISO events that occur outside of the target months. In the updated version, we use the extended winter (DJFMA) and summer (JJASO) to derive the EEOFs that define the MJO and the BSISO modes, respectively. Although this modification gives rise to only small differences in the EEOF patterns, the representation of the ISO seems to be improved throughout the year, leading to a more uniform distribution of the frequency of occurrence of significant ISO days across months. Also the average frequency of occurrence of significant ISO days slightly increases, which is now more in line with other ISO indices. It should be emphasized, however, that the original and the updated versions of the ISO index are highly consistent and most results would be insensitive to the choice of either version to be used.

Using the JRA-55 OLR, the bimodal ISO index was extended back in time to 1958. The same procedures are employed to construct the index. Despite large biases seen in the climatological mean and intraseasonal variability in OLR (Fig. 6), the JRA-55-based ISO index is remarkably consistent with the observation-based index. A comparison between JRA-55 and JRA-55C lends confidence in the reliability of the index even in the pre-satellite era (prior to 1972).

It is hoped that the new, extended, JRA-55-based bimodal ISO index will enhance a number of future studies. We anticipate that we could address more rigorously certain aspects of the ISO per se such as its interannual and multidecadal variability. As discussed in Section 4.5, our understanding of what controls the year-to-year variability of ISO activity is still incomplete. In addition, given its profound influence on other phenomena of a wide range of space-time scales such as TC genesis, tropical-extratropical interactions, etc., the index would be useful to examine whether and how the relationship between the ISO and other phenomenon varies over the last six decades.

The results of this study encourage further extensions of the index using longer-term reanalysis. Currently, several types of reanalysis that covers the entire twentieth century are available; the twentieth-century reanalysis project (20CR; Compo et al. 2011), the ECMWF twentieth century reanalysis (ERA-20C; Poli et al. 2016), and CERA-20C (Laloyaux et al. 2016). These are based on assimilation of only early instrumental record such as surface pressure and marine wind observations. Using such reanalysis, some studies reconstructed RMM-based ISO indices over the course of the 20th century (Oliver and Thompson 2012; Poli et al. 2016) and showed that these indices capture the ISO variability relatively well at least in the last three decades. Perhaps, these long-term reanalysis datasets would provide excellent opportunities to rigorously investigate various aspects of the ISO, in particular linear trends. Estimating linear trends reliably, however, seem to be challenging (Oliver 2016 and also as discussed in Section 4.5). Presumably, using synergistically these reanalysis datasets, efforts to construct a best reliable estimate of the bimodal ISO index and to assess its uncertainties over the course of the 20th century is a worthwhile direction of future work.

Acknowledgement

This research was supported by NOAA Grant NA17OAR4310250. Additional support was provided by the JAMSTEC through its sponsorship of research activities at the IPRC (JICS). The JRA-55 datasets are provided by the JMA. Interpolated OLR data provided by the NOAA/OAR/ESRL PSD, Boulder, Colorado, USA, from their Web site at https://www.esrl.noaa.gov/psd/. I thank Dr. Hironori Fudeyasu for encouraging me to conduct this study and for his comments on an earlier version of this manuscript. Thanks also goes to Dr. Ryuji Yoshida for his comments on an earlier version of this manuscript. Invaluable comments from three anonymous reviewers are also greatly appreciated to improve the manuscript.

References

Cassou, C., 2008: Intraseasonal interaction between the Madden-Julian Oscillation and the North Atlantic Oscillation. *Nature*, **455,** 523-527**,** doi:10.1038/nature07286.

Compo, G. P., J. S. Whitaker, P. D. Sardeshmukh, N. Matsui, R. J. Allan, X. Yin, B. E. Gleason, R. S. Vose, G. Rutledge, P. Bessemoulin, S. Bronnimann, M. Brunet, R. I. Crouthamel, A. N. Grant, P. Y. Groisman, P. D. Jones, M. C. Kruk, A. C. Kruger, G. J. Marshall, M. Maugeri, H. Y. Mok, O. Nordli, T. F. Ross, R. M. Trigo, X. L. Wang, S. D. Woodruff, and S. J. Worley, 2011: The twentieth century reanalysis project. *Quart. J. Roy. Met. Soc.*, **137,** 1-28

Duchon, C. E., 1979: Lanczos filtering in one and two dimensions. *J. Appl. Meteorol.*, **18,** 1016-1022

Emery, W. J. and R. E. Thomson, 1997: *Data analysis methods in physical oceanography*. Elsevier.

Folland, C. K., 1999: Large scale modes of ocean surface temperature since the late nineteenth century. *Beyond El Nino: decadal and interdecadal climate variability*, A. Navarra, Ed., Springer, New York, 73-102.

Gottschalck, J., P. E. Roundy, C. J. Schreck, A. Vintzileos, and C. D. Zhang, 2013: Large-scale atmospheric and oceanic conditions during the 2011-12 DYNAMO field campaign. *Mon. Wea. Rev.*, **141,** 4173-4196**,** doi:10.1175/mwr-d-13-00022.1.

Harada, Y., H. Kamahori, C. Kobayashi, H. Endo, S. Kobayashi, Y. Ota, H. Onoda, K. Onogi, K. Miyaoka, and K. Takahashi, 2016: The JRA-55 reanalysis: Representation of atmospheric circulation and climate variability. *J. Meteor. Soc. Japan*, **94,** 269-302**,** doi:10.2151/jmsj.2016-015.

Hendon, H. H., C. D. Zhang, and J. D. Glick, 1999: Interannual variation of the Madden-Julian oscillation during austral summer. *J. Climate*, **12,** 2538-2550

Hendon, H. H., M. C. Wheeler, and C. D. Zhang, 2007: Seasonal dependence of the MJO-ENSO relationship. *J. Climate*, **20,** 531-543

Henley, B. J., J. Gergis, D. J. Karoly, S. Power, J. Kennedy, and C. K. Folland, 2015: A tripole index for the interdecadal Pacific oscillation. *Clim. Dyn.*, **45,** 3077-3090**,** doi:10.1007/s00382-015-2525-1.

Hirata, H. and R. Kawamura, 2014: Scale interaction between typhoons and the North Pacific subtropical high and associated remote effects during the Baiu/Meiyu season. *J. Geophys. Res. Atmos.*, **119,** 5157-5170**,** doi:10.1002/2013jd021430.

Huang, B. Y., P. W. Thorne, V. F. Banzon, T. Boyer, G. Chepurin, J. H. Lawrimore, M. J. Menne, T. M. Smith, R. S. Vose, and H. M. Zhang, 2017: Extended reconstructed sea surface temperature, version 5 (ersstv5): Upgrades, validations, and intercomparisons. *J. Climate*, **30,** 8179-8205**,** doi:10.1175/jcli-d-16-0836.1.

Johnson, R. H., P. E. Ciesielski, J. H. Ruppert, Jr., and M. Katsumata, 2015: Sounding-based thermodynamic budgets for DYNAMO. *J. Atmos. Sci.*, **72,** 598-622**,** doi:10.1175/jas-d-14-0202.1.

Jones, C. and L. M. V. Carvalho, 2006: Changes in the activity of the Madden-Julian Oscillation during 1958-2004. *J. Climate*, **19,** 6353-6370**,** doi:10.1175/jcli3972.1.

Kalnay, E., M. Kanamitsu, R. Kistler, W. Collins, D. Deaven, L. Gandin, M. Iredell, S. Saha, G. White, J. Woollen, Y. Zhu, M. Chelliah, W. Ebisuzaki, W. Higgins, J. Janowiak, K. C. Mo, C. Ropelewski, J. Wang, A. Leetmaa, R. Reynolds, R. Jenne, and D. Joseph, 1996: The NCEP/NCAR 40-year reanalysis project. *Bull. Amer. Meteor. Soc.*, **77,** 437-471

Kanamitsu, M., W. Ebisuzaki, J. Woollen, S. K. Yang, J. J. Hnilo, M. Fiorino, and G. L. Potter, 2002: NCEP-DOE AMIP-II reanalysis (R-2). *Bull. Amer. Meteor. Soc.*, **83,** 1631-1643

Kikuchi, K., B. Wang, and Y. Kajikawa, 2012: Bimodal representation of the tropical intraseasonal oscillation. *Clim. Dyn.*, **38,** 1989-2000**,** doi:10.1007/s00382-011-1159-1.

Kikuchi, K., G. N. Kiladis, J. Dias, and T. Nasuno, 2018: Convectively coupled equatorial waves within the MJO during CINDY/DYNAMO: slow Kelvin waves as building blocks. *Clim. Dyn.*, **50,** 4211-4230**,** doi:10.1007/s00382-017-3869-5.

Kikuchi, K., C. Kodama, T. Nasuno, M. Nakano, H. Miura, M. Satoh, A. T. Noda, and Y. Yamada, 2017: Tropical intraseasonal oscillation simulated in an AMIP-type experiment by NICAM. *Clim. Dyn.*, **48,** 2507-2528**,** doi:10.1007/s00382-016-3219-z.

Kiladis, G. N., J. Dias, K. H. Straub, M. C. Wheeler, S. N. Tulich, K. Kikuchi, K. M. Weickmann, and M. J. Ventrice, 2014: A comparison of olr and circulation-based indices for tracking the MJO. *Mon. Wea. Rev.*, **142,** 1697-1715**,** doi:10.1175/mwr-d-13-00301.1.

Kim, D., K. Sperber, W. Stern, D. Waliser, I. S. Kang, E. Maloney, W. Wang, K. Weickmann, J. Benedict, M. Khairoutdinov, M. I. Lee, R. Neale, M. Suarez, K. Thayer-Calder, and G. Zhang, 2009: Application of MJO simulation diagnostics to climate models. *J. Climate*, **22,** 6413-6436**,** doi:10.1175/2009jcli3063.1.

Kim, H., F. Vitart, and D. E. Waliser, 2018: Precition of the Madden-Julian oscillation: A review. *J. Climate Appl. Meteor.*, **31,** 9425-9443**,** doi:10.1175/JCLI-D-18-0210.1.

Klotzbach, P. J., S. Abhik, H. H. Hendon, M. Bell, C. Lucas, A. G. Marshall, and E. C. J. Oliver, 2019: On the emerging relationship between the stratospheric quasi-biennial oscillation and the Madden-Julian oscillation. *Scientific Reports*, doi:10.1038/s41598-019-40034-6.

Knutson, T. R. and K. M. Weickmann, 1987: 30-60 day atmospheric oscillations: Composite life-cycles of convection and circulation anomalies. *Mon. Wea. Rev.*, **115,** 1407-1436

Kobayashi, C., H. Endo, Y. Ota, S. Kobayashi, H. Onoda, Y. Harada, K. Onogi, and H. Kamahori, 2014: Preliminary results of the JRA-55C, an atmospheric reanalysis assimilating conventional observations only. *Sola*, **10,** 78-82**,** doi:10.2151/sola.2014-016.

Kobayashi, S., Y. Ota, Y. Harada, A. Ebita, M. Moriya, H. Onoda, K. Onogi, H. Kamahori, C. Kobayashi, H. Endo, K. Miyaoka, and K. Takahashi, 2015: The JRA-55 reanalysis: general specifications and basic characteristics. *J. Meteor. Soc. Japan*, **93,** 5-48**,** doi:10.2151/jmsj.2015-001.

Konda, G. and N. K. Vissa, 2019: Intraseasonal convection and air–sea fluxes over the Indian monsoon region revealed from the Bimodal ISO index. *Pure and Applied Geophysics***,** doi:10.1007/s00024-019-02119-1.

Laloyaux, P., M. Balmaseda, D. Dee, K. Mogensen, and P. Janssen, 2016: A coupled data assimilation system for climate reanalysis. *Quart. J. Roy. Met. Soc.*, **142,** 65-78**,** doi:10.1002/qj.2629.

Lau, K. M. and P. H. Chan, 1985: Aspects of the 40-50 day oscillation during the northern winter as inferred from outgoing longwave radiation. *Mon. Wea. Rev.*, **113,** 1889-1909

Lau, K. M. and P. H. Chan, 1986: Aspects of the 40-50 day oscillation during the northern summer as inferred from outgoing longwave radiation. *Mon. Wea. Rev.*, **114,** 1354-1367

Lau, W. K. M. and D. Waliser, Eds., 2012: *Intraseasonal Variability in the Atmosphere–Ocean Climate System*. 2nd ed. Springer, 614 pp.

Liebmann, B. and C. A. Smith, 1996: Description of a complete (interpolated) outgoing longwave radiation dataset. *Bull. Amer. Meteor. Soc.*, **77,** 1275-1277

Liu, P., Q. Zhang, C. D. Zhang, Y. J. Zhu, M. Khairoutdinov, H. M. Kim, C. Schumacher, and M. H. Zhang, 2016: A revised real-time multivariate MJO index. *Mon. Wea. Rev.*, **144,** 627-642**,** doi:10.1175/mwr-d-15-0237.1.

Madden, R. A. and P. R. Julian, 1971: Detection of a 40-50 day oscillation in the zonal wind in the tropical Pacific. *J. Atmos. Sci.*, **28,** 702-708

Madden, R. A. and P. R. Julian, 1972: Description of global-scale circulation cells in tropics with a 40-50 day period. *J. Atmos. Sci.*, **29,** 1109-1123

Madden, R. A. and P. R. Julian, 1994: Observations of the 40-50-day tropical oscillation: A review. *Mon. Wea. Rev.*, **122,** 814-837

Nakano, M. and K. Kikuchi, 2019: Seasonality of intraseasonal variability in CMIP5 and a nonhydrostatic atmospheric global models. *Geophys. Res. Lett.***,** doi:10.1029/2019GL082443.

Oliver, E. C. J., 2016: Blind use of reanalysis data: apparent trends in Madden-Julian Oscillation activity driven by observational changes. *Int. J. Climatol.*, **36,** 3458-3468**,** doi:10.1002/joc.4568.

Oliver, E. C. J. and K. R. Thompson, 2012: A reconstruction of Madden-Julian oscillation variability from 1905 to 2008. *J. Climate*, **25,** 1996-2019**,** doi:10.1175/jcli-d-11-00154.1.

Onogi, K., J. Tslttsui, H. Koide, M. Sakamoto, S. Kobayashi, H. Hatsushika, T. Matsumoto, N. Yamazaki, H. Kaalhori, K. Takahashi, S. Kadokura, K. Wada, K. Kato, R. Oyama, T. Ose, N. Mannoji, and R. Taira, 2007: The JRA-25 reanalysis. *J. Meteor. Soc. Japan*, **85,** 369-432

Pang, B., Z. S. Chen, Z. P. Wen, and R. Y. Lu, 2016: Impacts of two types of El Nio on the MJO during boreal winter. *Advances in Atmospheric Sciences*, **33,** 979-986**,** doi:10.1007/s00376-016-5272-2.

Poli, P., H. Hersbach, D. P. Dee, P. Berrisford, A. J. Simmons, F. Vitart, P. Laloyaux, D. G. H. Tan, C. Peubey, J. N. Thepaut, Y. Tremolet, E. V. Holm, M. Bonavita, L. Isaksen, and M. Fisher, 2016: ERA-20C: An atmospheric reanalysis of the twentieth century. *J. Climate*, **29,** 4083-4097**,** doi:10.1175/jcli-d-15-0556.1.

Power, S., T. Casey, C. Folland, A. Colman, and V. Mehta, 1999: Inter-decadal modulation of the impact of ENSO on Australia. *Clim. Dyn.*, **15,** 319-324**,** doi:10.1007/s003820050284.

Santer, B. D., T. M. L. Wigley, J. S. Boyle, D. J. Gaffen, J. J. Hnilo, D. Nychka, D. E. Parker, and K. E. Taylor, 2000: Statistical significance of trends and trend differences in layer-average atmospheric temperature time series. *J. Geophys. Res. Atmos.*, **105,** 7337-7356**,** doi:10.1029/1999jd901105.

Serra, Y. L., X. A. Jiang, B. J. Tian, J. Amador-Astua, E. D. Maloney, and G. N. Kiladis, 2014: Tropical intraseasonal modes of the atmosphere. *Annual Review of Environment and Resources, Vol 39*, A. Gadgil and D. M. Liverman, Eds., 189-215.

Shibuya, R., M. Nakano, C. Kodama, T. Nasuno, M. Satoh, T. Miyakawa, H. Miura, and K. Kikuchi, 2018: Prediction skill of the boreal summer intra-seasonal oscillation in a global cloud-system resolving simulation. *J. Adv. Model. Earth Syst.***,** in preparation

Slingo, J. M., D. P. Rowell, K. R. Sperber, and E. Nortley, 1999: On the predictability of the interannual behaviour of the Madden-Julian Oscillation and its relationship with El Nino. *Quart. J. Roy. Met. Soc.*, **125,** 583-609

Son, S. W., Y. Lim, C. H. Yoo, H. H. Hendon, and J. Kim, 2017: Stratospheric control of the Madden-Julian Oscillation. *J. Climate*, **30,** 1909-1922**,** doi:10.1175/jcli-d-16-0620.1.

Straub, K. H., 2013: MJO Initiation in the real-time multivariate MJO index. *J. Climate*, **26,** 1130-1151**,** doi:10.1175/jcli-d-12-00074.1.

Szekely, E., D. Giannakis, and A. J. Majda, 2016: Extraction and predictability of coherent intraseasonal signals in infrared brightness temperature data. *Clim. Dyn.*, **46,** 1473-1502**,** doi:10.1007/s00382-015-2658-2.

Torrence, C. and G. P. Compo, 1998: A practical guide to wavelet analysis. *Bull. Amer. Meteor. Soc.*, **79,** 61-78

Uppala, S. M., P. W. Kallberg, A. J. Simmons, U. Andrae, V. D. Bechtold, M. Fiorino, J. K. Gibson, J. Haseler, A. Hernandez, G. A. Kelly, X. Li, K. Onogi, S. Saarinen, N. Sokka, R. P. Allan, E. Andersson, K. Arpe, M. A. Balmaseda, A. C. M. Beljaars, L. Van De Berg, J. Bidlot, N. Bormann, S. Caires, F. Chevallier, A. Dethof, M. Dragosavac, M. Fisher, M. Fuentes, S. Hagemann, E. Holm, B. J. Hoskins, L. Isaksen, P. Janssen, R. Jenne, A. P. McNally, J. F. Mahfouf, J. J. Morcrette, N. A. Rayner, R. W. Saunders, P. Simon, A. Sterl, K. E. Trenberth, A. Untch, D. Vasiljevic, P. Viterbo, and J. Woollen, 2005: The ERA-40 re-analysis. *Quart. J. Roy. Met. Soc.*, **131,** 2961-3012**,** doi:10.1256/qj.04.176.

Ventrice, M. J., M. C. Wheeler, H. H. Hendon, C. J. Schreck, III, C. D. Thorncroft, and G. N. Kiladis, 2013: A modified multivariate Madden-Julian oscillation index using velocity potential. *Mon. Wea. Rev.*, **141,** 4197-4210**,** doi:10.1175/mwr-d-12-00327.1.

Wang, B. and H. Rui, 1990: Synoptic climatology of transient tropical intraseasonal convection anomalies: 1975-1985. *Meteor. Atmos. Phys.*, **44,** 43-61

Wang, L., T. Li, L. Chen, S. K. Behera, and T. Nasuno, 2018a: Modulation of the MJO intensity over the equatorial western Pacific by two types of El Nino. *Clim. Dyn.*, **51,** 687-700**,** doi:10.1007/s00382-017-3949-6.

Wang, S., D. Ma, A. H. Sobel, and M. K. Tippett, 2018b: Propagation characteristics of BSISO Indices. *Geophys. Res. Lett.***,** doi:10.1029/2018GL078321.

Weare, B. C. and J. S. Nasstrom, 1982: Examples of extended empirical orthogonal function analyses. *Mon. Wea. Rev.*, **110,** 481-485

Wheeler, M. C. and H. H. Hendon, 2004: An all-season real-time multivariate MJO index: Development of an index for monitoring and prediction. *Mon. Wea. Rev.*, **132,** 1917-1932

Wheeler, M. C., H. H. Hendon, S. Cleland, H. Meinke, and A. Donald, 2009: Impacts of the Madden-Julian Oscillation on Australian rainfall and circulation. *J. Climate*, **22,** 1482-1498**,** doi:10.1175/2008jcli2595.1.

Wolter, K. and M. S. Timlin, 1993: Monitoring ENSO in COADS with a seasonally adjusted principal component index. *Proc. of the 17th Climate Diagnostics Workshop*, Norman, OK, NOAA/NMC/CAC, NSSL, Oklahoma Clim. Survey, CIMMS and the School of Meteor., Univ. of Oklahoma, 52-57.

Wolter, K. and M. S. Timlin, 1998: Measuring the strength of ENSO events - how does 1997/98 rank? *Weather*, **53,** 315-324

Yamaura, T. and Y. Kajikawa, 2017: Decadal change in the boreal summer intraseasonal oscillation. *Clim. Dyn.*, **48,** 3003-3014**,** doi:10.1007/s00382-016-3247-8.

Yasunari, T., 1979: Cloudiness fluctuations associated with the northern hemisphere summer monsoon. *J. Meteor. Soc. Japan*, **57,** 227-242

Yoneyama, K., C. Zhang, and C. N. Long, 2013: Tracking pulses of the Madden-Julian oscillation. *Bull. Amer. Meteor. Soc.*, **94,** 1871-1891**,** doi:10.1175/bams-d-12-00157.1.

Yoo, C. and S.-W. Son, 2016: Modulation of the boreal wintertime Madden-Julian oscillation by the stratospheric quasi-biennial oscillation. *Geophys. Res. Lett.*, **43,** 1392-1398**,** doi:10.1002/2016GL067762.

Yoshida, R., Y. Kajikawa, and H. Ishikawa, 2014: Impact of boreal summer intraseasonal oscillation on environment of tropical cyclone genesis over the western North Pacific. *Sola*, **10,** 15-18**,** doi:10.2151/sola.2014-004.

Zhang, C. D., 2013: Madden-Julian oscillation: Bridging weather and climate. *Bull. Amer. Meteor. Soc.*, **94,** 1849-1870**,** doi:10.1175/bams-d-12-00026.1.

Table and Figure captions

Table 1 Correlations between the original and updated versions in EEOFs and corresponding PCs. Pattern correlations are calculated between the original (based on 1979-2009 summer and winter seasons) and updated (1979-January 2017 extended summer and winter seasons) versions in the first two EEOFs and lagged correlations between the original and updated versions in the first two PCs. Numbers in brackets denote lags in day at which the maximum correlations occur and positive values mean the PC of the updated version lags that of the original.

Table 2 Same as Table 1 except for between the observed and JRA-55

Table 3 Same as Table 1 except for between JRA-55 and JRA-55C

Table 4 Correlations of the seasonal mean ISO amplitudes with ENSO and the QBO on the interannual timescale based on the period 1958-2017. The state of ENSO is represented by multivariate ENSO index (MEI; Wolter and Timlin 1993, 1998). The state of the QBO is measured by zonal-mean zonal wind, averaged over 10ºN–10ºS, at 10 hPa (U10), 20 hPa (U20), 30 hPa (U30), and 50 hPa (U50). Statistically significant values at the 95% confidence levels are indicated by bold-faced type.

Fig. 1. Flowchart summarizing the procedure for identifying significant ISO events in terms of the MJO mode and the BSISO mode. $A^* = (PC_1^{*2} + PC_2^{*2})^{1/2}$ and $A = (PC_1^2 + PC_2^2)^{1/2}$ is the normalized and non-normalized amplitude, respectively, of either the MJO or BSISO mode, where PC^* represents the normalized PC by one standard deviation during the period the EEOF analysis was performed. Adapted from Kikuchi et al. (2012).

Fig. 2 Evolution of the ISO convection patterns during boreal winter (left) and summer (right) represented in terms of the first two EEOFs of intraseasonal (25–90 day) OLR anomalies. The EEOFs in the left and right panels are calculated using (top) DJF and JJA data, respectively, for the period 1979–2009 and (bottom) DJFMA and JJASO for the period 1979-January 2017, which are used to define the MJO and BSISO modes, respectively. The contribution of each EEOF mode to total variance is denoted above each panel. Note that the pair of the first two EEOFs represents a half of the life cycle of each ISO mode.

Fig. 3 A comparison of the ISO index between the (upper panels) original and (lower panels) updated versions for the MJO and the BSISO modes, respectively for the year 2001. Note that each PC is normalized by one standard deviation of the corresponding PCs during the period each EEOF analysis was performed to obtain the EEOFs. Significant ISO events are shaded in the background.

Fig. 4 Climatological annual cycle of the normalized amplitudes of the MJO mode (blue) and the BSISO mode (red). The original and updated version are represented by dashed and solid lines, respectively.

Fig. 5 Frequency of occurrence of significant ISO days as a function of calendar month normalized by the number of days available each month for the (a) original and (b) updated versions.

Fig. 6 Annual mean climatological OLR (left) and standard deviation of intraseasonal (25-90 day) OLR anomalies in W m^{-2} based on (left) NOAA interpolated and (right) JRA-55.

Fig. 7 Same as Fig. 1b and d except for JRA-55 for the period 1958-2017. Note that the contour interval is halved.

Fig. 8 Snapshots of OLR on 27 October 2011 for (a) observation, (b) JRA-55, and (c) JRA-55C.

Fig. 9 Same as Fig. 5 except for those derived from JRA-55C.

Fig. 10 Same as Fig. 3 except for the JRA-55 for the period 1958-2017 (color bars) in conjunction with that for the period 1958-2017 based on the JRA-55 (black line) and the observation (i.e., Fig. 5b, green line).

Fig. 11 Composite life cycle of the MJO mode for (a) observation and (b) JRA-55 in terms of OLR anomalies. Significant values at the 99 % level according to the t test with degree of freedom being one sixth of the number of composite samples (taking account of persistence) are only drawn.

Fig. 12 Same as Fig. 11 except for the BSISO mode.

Fig. 13 Time series of 91-day running mean $\mathrm{PC}_1^2 + \mathrm{PC}_2^2$, showing the low-frequency (primarily interannual) modulation of the variance of the MJO mode (blue) and the BSISO mode (red).

Fig. 14 The local wavelet power spectrum of the 3 month running mean (a) MJO and (b) BSISO amplitudes. The left axis is the Fourier period (in yr) corresponding to the wavelet scale on the right axis. The bottom axis is time (yr). The green contour encloses regions of greater than 90% confidence for a red-noise process with a lag-1 coefficient. The cone of influence is indicated by the thick curved lines.

Fig. 15 Correlations between the BSISO activity and SST anomalies during JJA on (a) interannual (4-8 years) and (b) interdecadal (longer than 13 years) timescales. Anomalies on the interannual and interdecadal timescales are isolated, after removing the linear trend, by retaining the 8-16th and 1-5th components of the Fourier transform, respectively. The green marks represent where the correlations are significant at the 90% confidence level.

Fig. 16 Time series of the (a) MJO and (b) BSISO modes in terms of $\mathrm{PC}_1^2 + \mathrm{PC}_2^2$ averaged over the specified months indicated. The values are linear trend ($decade^{-1}$) and those with asterisk denote 90% significance.

Table 1 Correlations between the original and updated versions in EEOFs and corresponding PCs. Pattern correlations are calculated between the original (based on 1979-2009 summer and winter seasons) and updated (1979-January 2017 extended summer and winter seasons) versions in the first two EEOFs and lagged correlations between the original and updated versions in the first two PCs. Numbers in brackets denote lags in day at which the maximum correlations occur and positive values mean the PC of the updated version lags that of the original.

	$EEOF_{1,2}$	$PC_{1,2}$
Winter	0.96, 0.95	0.99 (+1), 0.99 (+1)
Summer	0.96, 0.96	0.99 (+1), 0.99 (+1)

Table 2 Same as Table 1 except for between the observed and JRA-55

	$EEOF_{1,2}$	$PC_{1,2}$
Winter	0.89, 0.86	0.96 (+2), 0.97 (+2)
Summer	0.92, 0.88	0.96 (+1), 0.96 (+1)

Table 3 Same as Table 1 except for between JRA-55 and JRA-55C

	$EEOF_{1,2}$	$PC_{1,2}$
Winter	0.97, 0.96	0.98 (-1), 0.99 (-1)
Summer	0.96, 0.96	0.98 (0), 0.98 (0)

Table 4 Correlations of the seasonal mean ISO amplitudes with ENSO and the QBO on the interannual timescale based on the period 1958-2017. The state of ENSO is represented by multivariate ENSO index (MEI). The state of the QBO is measured by zonal-mean zonal wind, averaged over 10ºN–10ºS, at 10 hPa (U10), 20 hPa (U20), 30 hPa (U30), and 50 hPa (U50). Statistically significant values at the 95% confidence levels are indicated by bold-faced type.

		Winter		Summer	
		DJF	DJFMA	JJA	JJASO
ENSO	MEI	0.16	0.12	0.10	0.04
QBO	U10	**0.39**	**0.34**	-0.14	-0.15
	U20	0.20	0.21	-0.05	-0.11
	U30	-0.12	-0.06	0.01	-0.04
	U50	**-0.34**	**-0.32**	0.10	0.08

Fig. 1

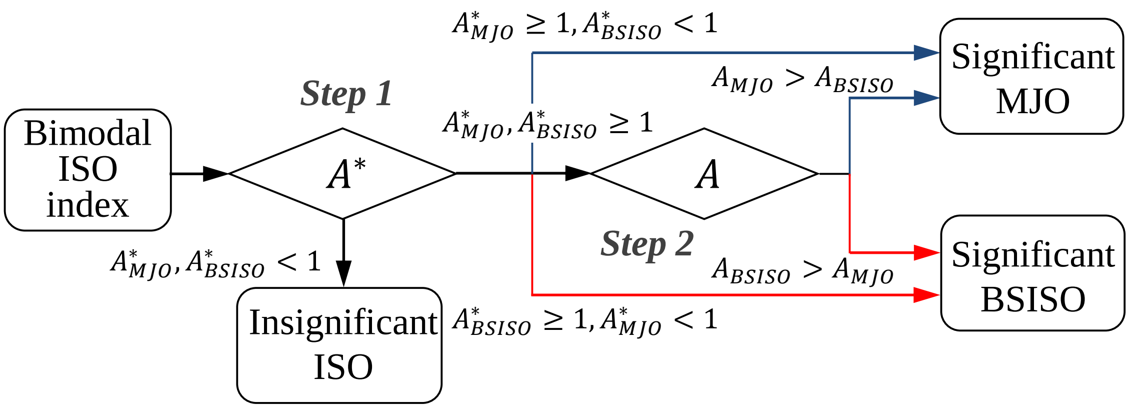

Fig. 1. Flowchart summarizes the procedure for identifying significant ISO events in terms of the MJO mode and the BSISO mode. $A^* = (PC_1^{*2} + PC_2^{*2})^{1/2}$ and $A = (PC_1^2 + PC_2^2)^{1/2}$ is the normalized and non-normalized amplitude, respectively, of either the MJO or BSISO mode, where PC^* represents the normalized PC by one standard deviation during the period the EEOF analysis was performed. Adapted from Kikuchi et al. (2012).

Fig. 2

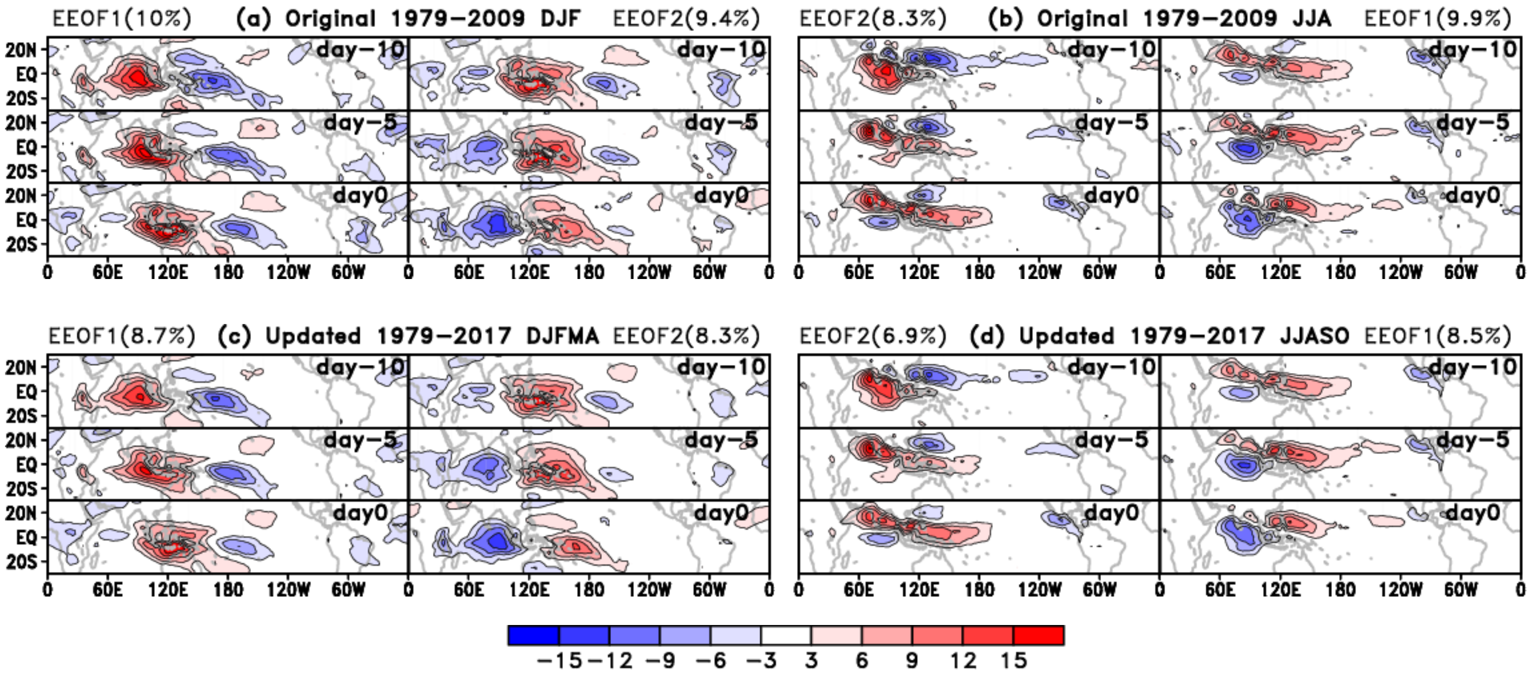

Fig. 2 Evolution of the ISO convection patterns during boreal winter (left) and summer (right) represented in terms of the first two EEOFs of intraseasonal (25–90 day) OLR anomalies. The EEOFs in the left and right panels are calculated using (top) DJF and JJA data, respectively, for the period 1979–2009 and (bottom) DJFMA and JJASO for the period 1979-January 2017, which are used to define the MJO and BSISO modes, respectively. The contribution of each EEOF mode to total variance is denoted above each panel. Note that the pair of the first two EEOFs represents a half of the life cycle of each ISO mode.

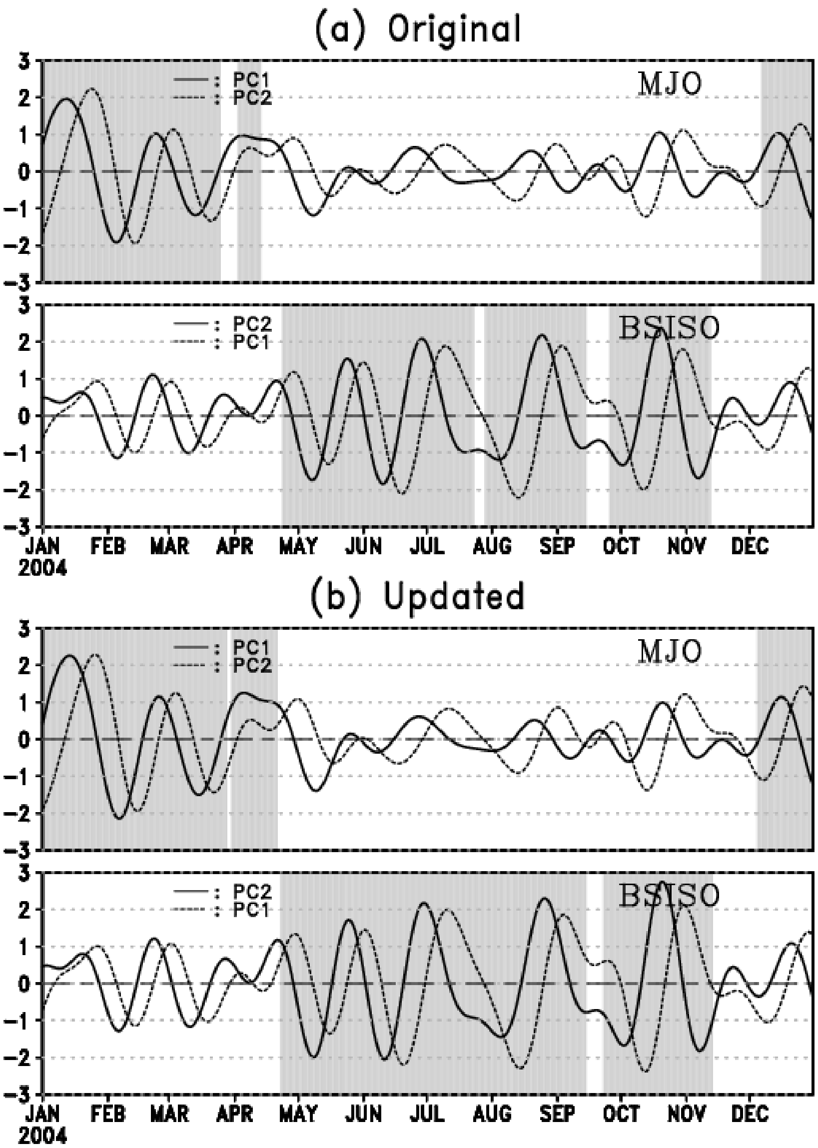

Fig. 3 A comparison of the ISO index between the (upper panels) original and (lower panels) updated versions for the MJO and the BSISO modes, respectively for the year 2001. Note that each PC is normalized by one standard deviation of the corresponding PCs during the period each EEOF analysis was performed to obtain the EEOFs. Significant ISO events are shaded in the background.

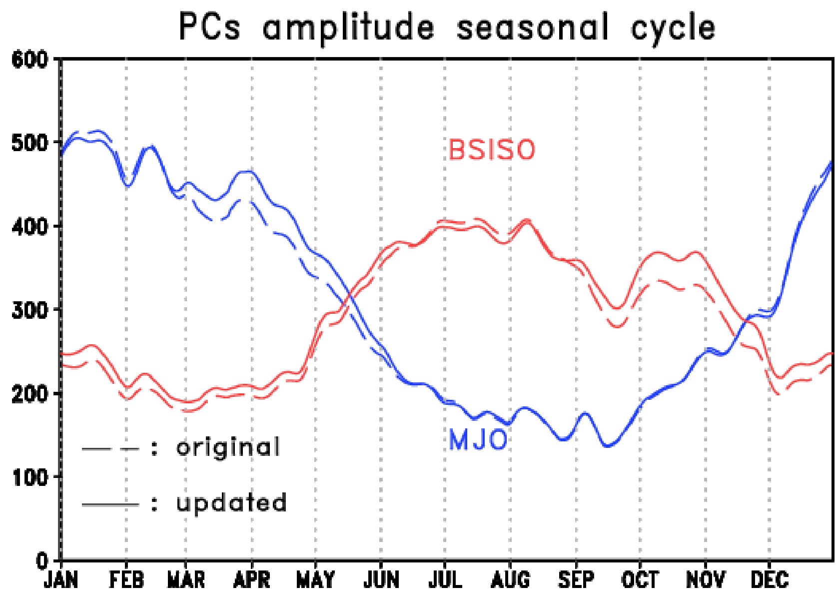

Fig. 4 Climatological annual cycle of the normalized amplitudes of the MJO mode (blue) and the BSISO mode (red). The original and updated version are represented by dashed and solid lines, respectively.

Fig. 5

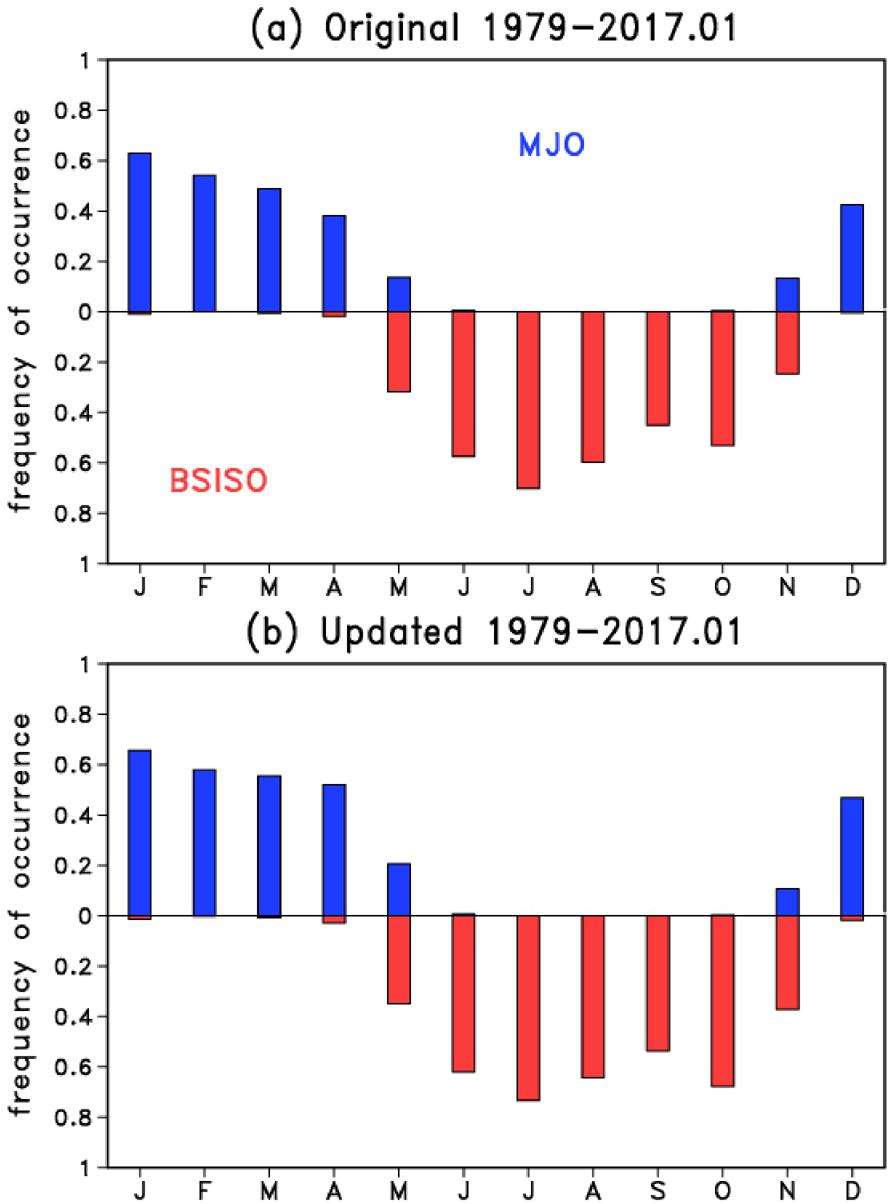

Fig. 5 Frequency of occurrence of significant ISO days as a function of calendar month normalized by the number of days available each month for the (a) original and (b) updated versions.

Fig. 6

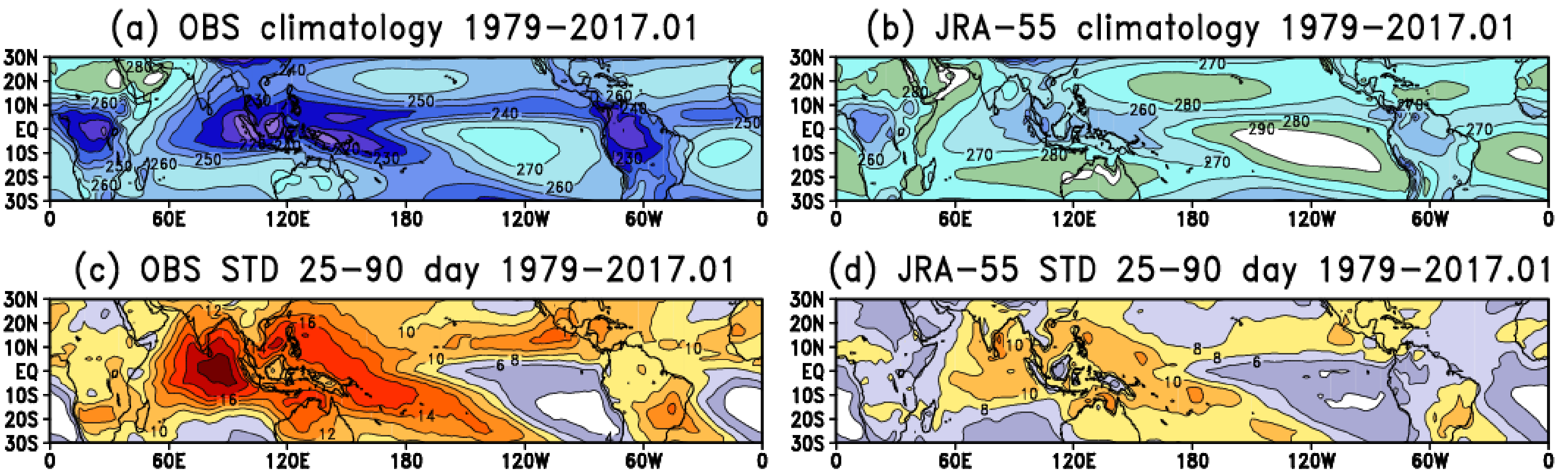

Fig. 6 Annual mean climatological OLR (top) and standard deviation of intraseasonal (25-90 day) OLR anomalies in W m^{-2} based on (left) NOAA interpolated and (right) JRA-55.

Fig. 7

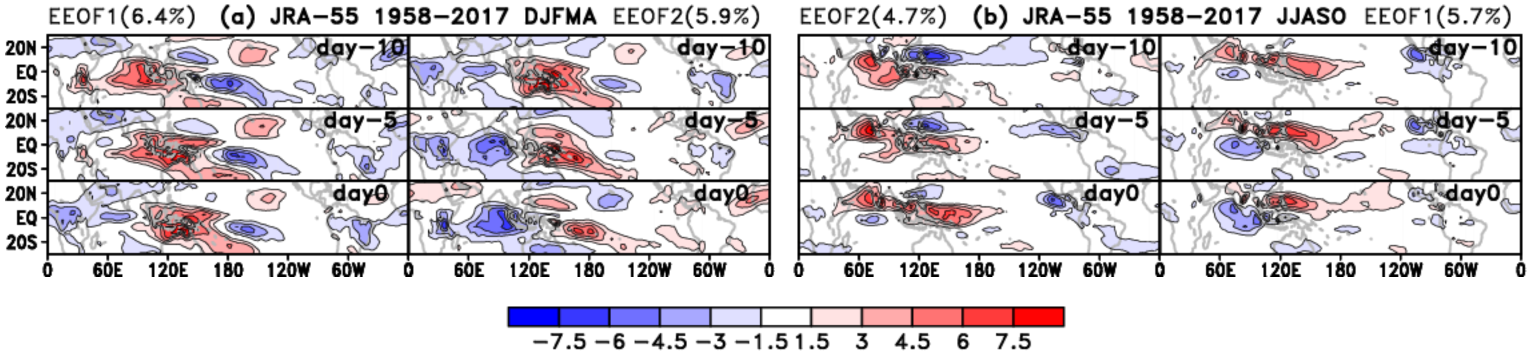

Fig. 7 Same as Fig. 1b and d except for JRA-55 for the period 1958-2017. Note that the contour interval is halved.

Fig. 8

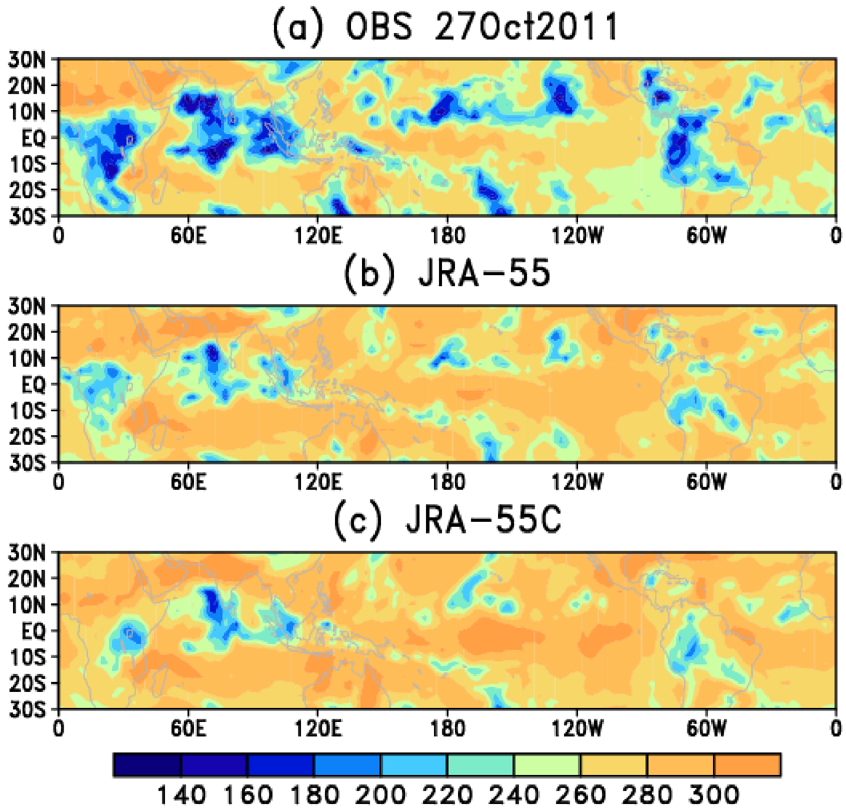

Fig. 8 Snapshots of OLR on 27 October 2011 for (a) observation, (b) JRA-55, and (c) JRA-55C.

Fig. 9

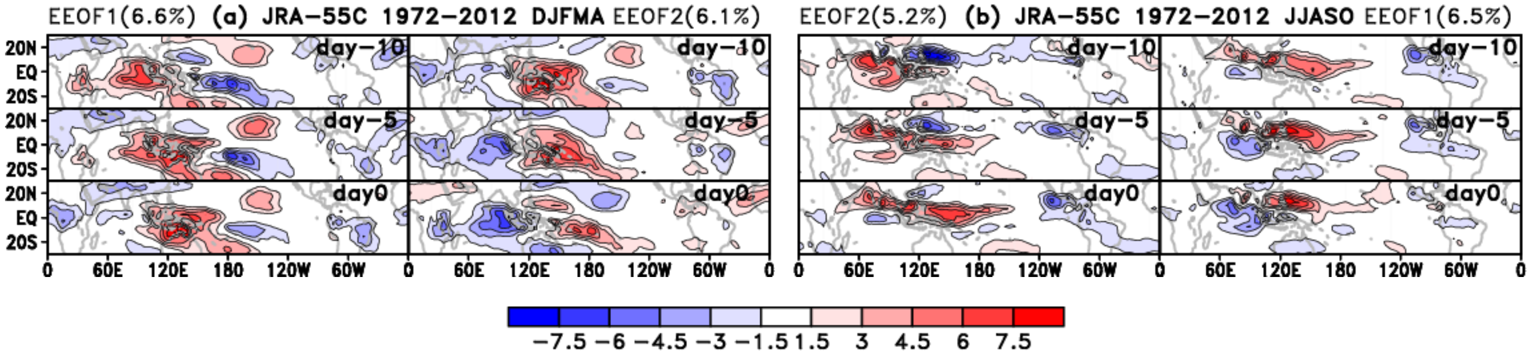

Fig. 9 Same as Fig. 5 except for those derived from JRA-55C.

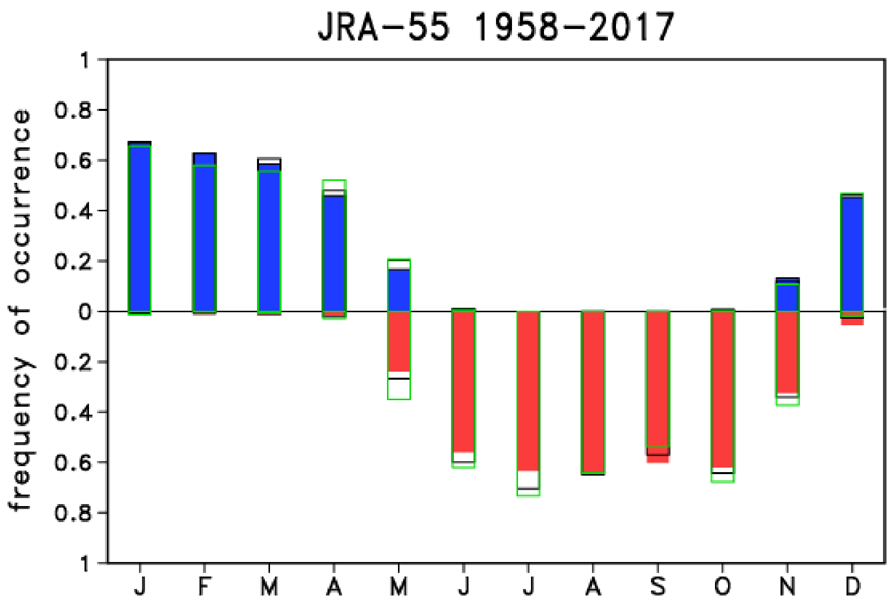

Fig. 10 Same as Fig. 5 except for the JRA-55 for the period 1958-2017 (color bars) in conjunction with that for the period 1979-2017 based on the JRA-55 and the observation (i.e., Fig. 5b, green line).

Fig. 11

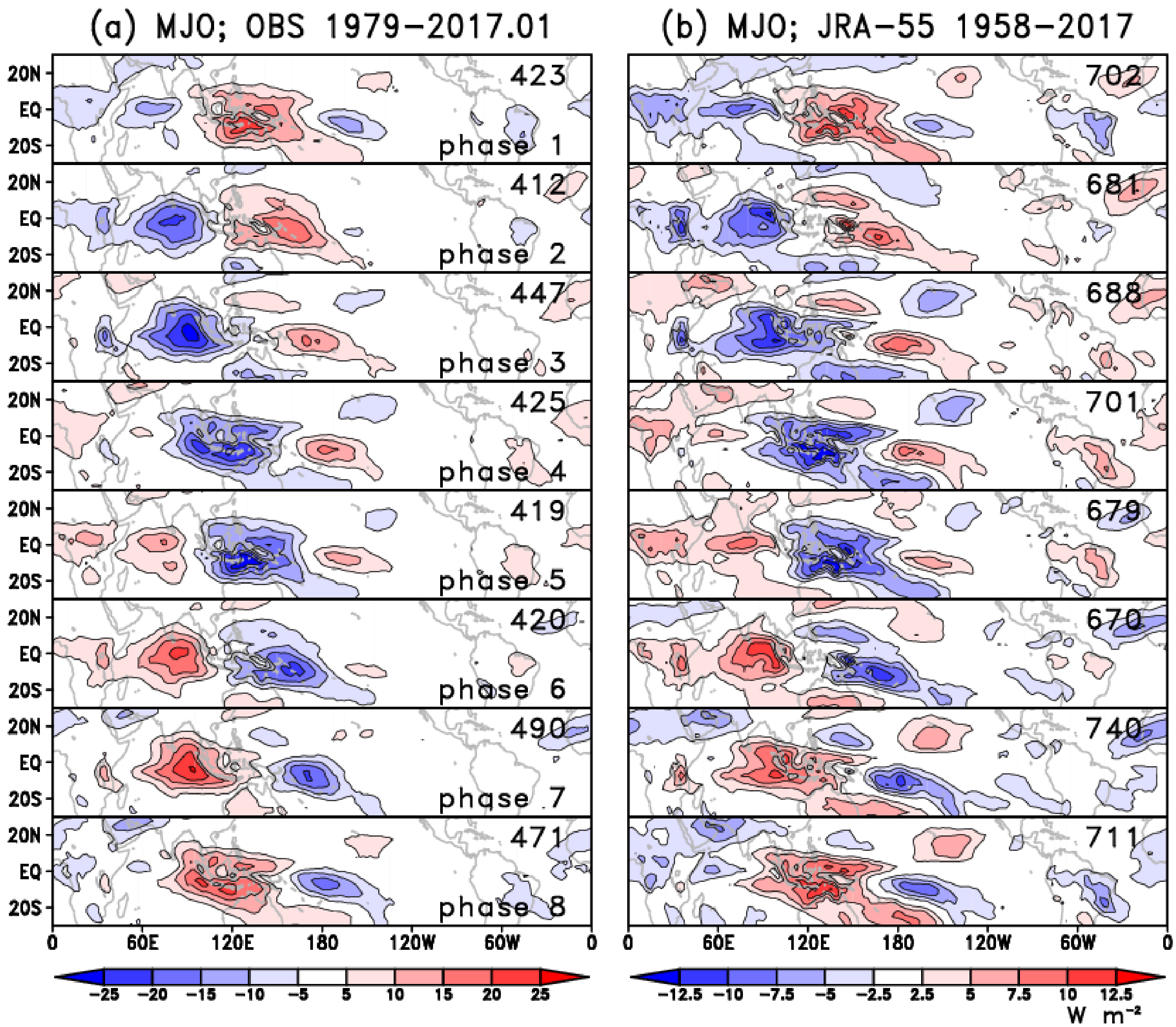

Fig. 11 Composite life cycle of the MJO mode for (a) observation and (b) JRA-55 in terms of OLR anomalies. Significant values at the 99 % level according to the t test with degree of freedom being one sixth of the number of composite samples (taking account of persistence) are only drawn.

Fig. 12

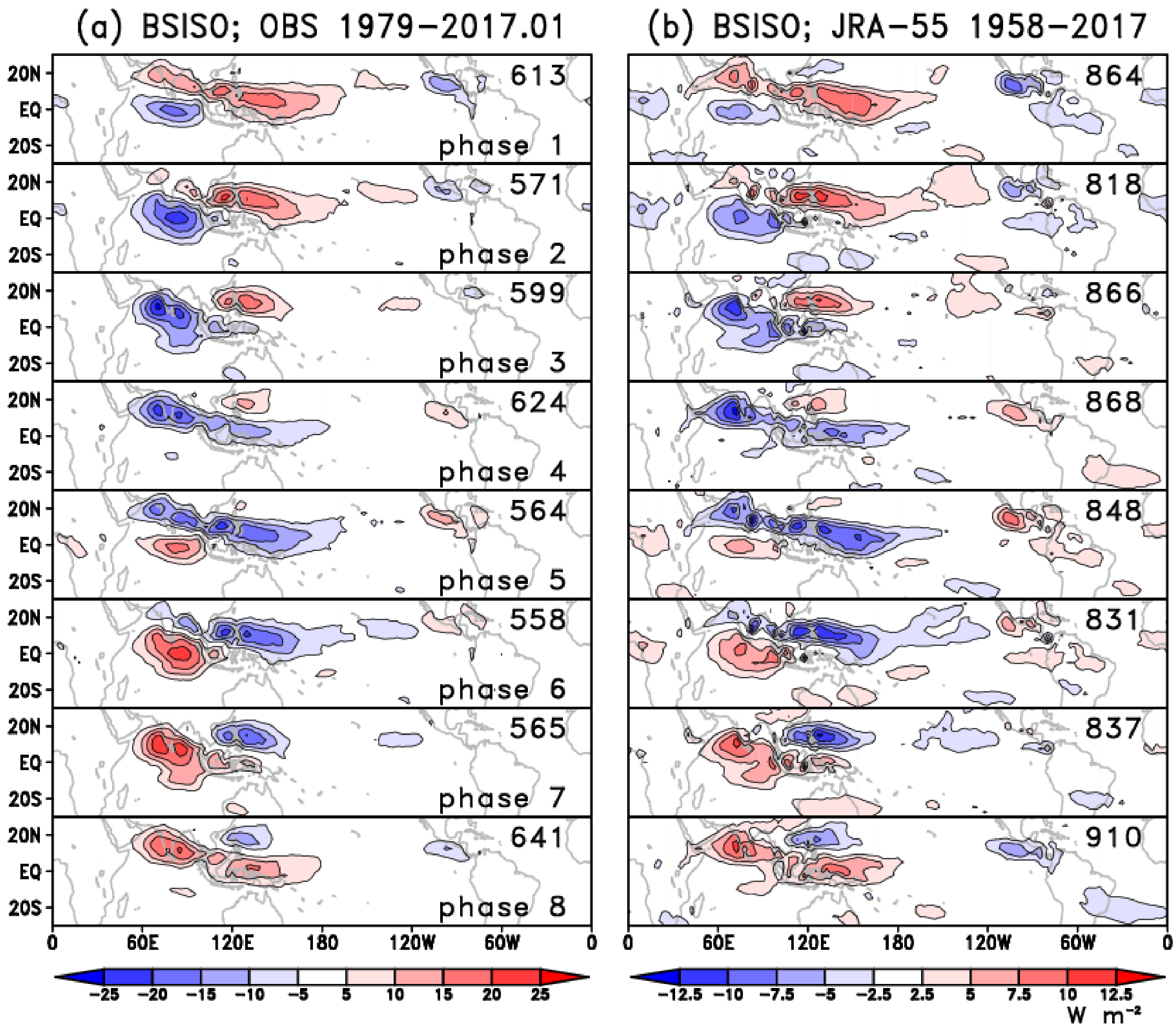

Fig. 12 Same as Fig. 11 except for the BSISO mode.

Fig. 13

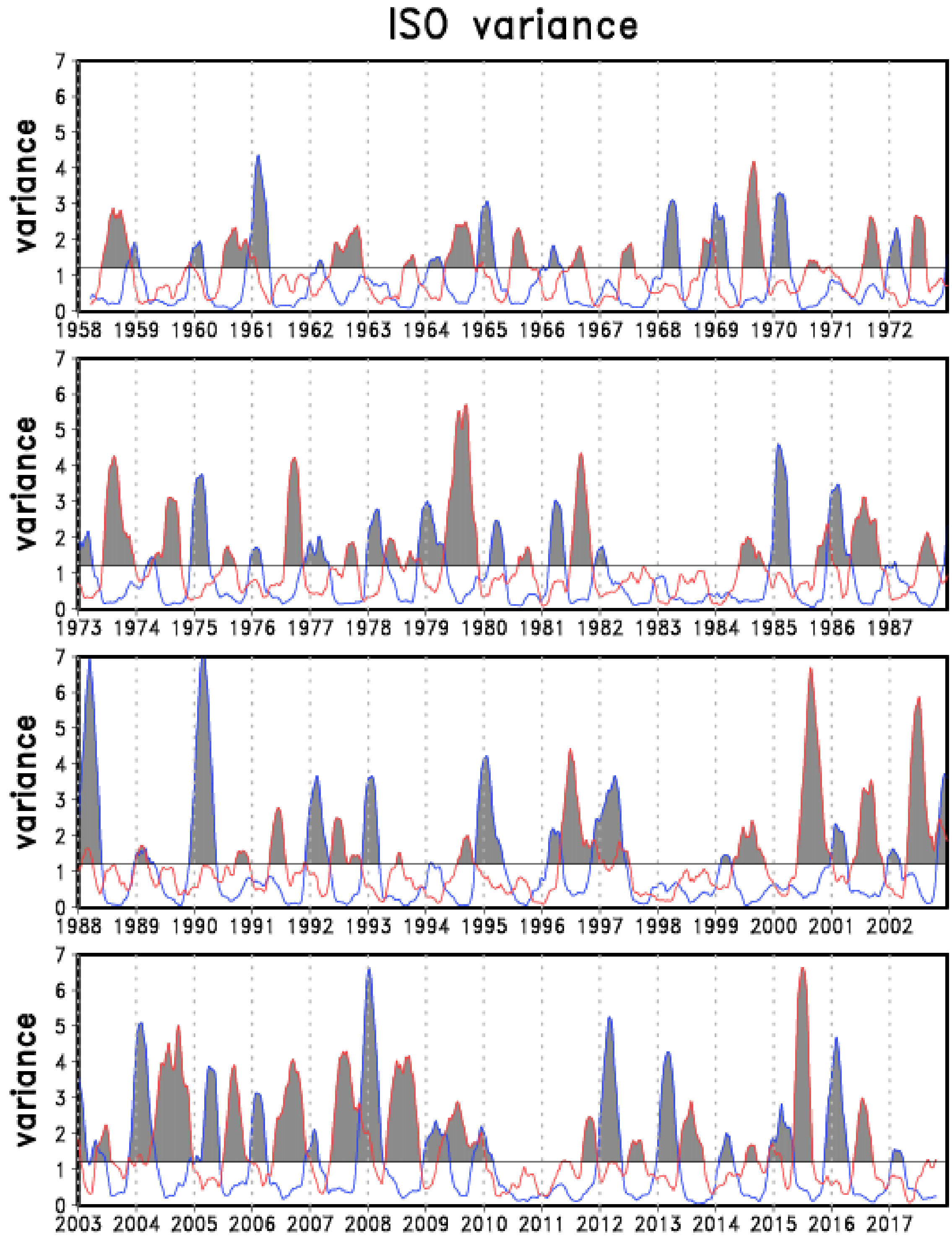

Fig. 13 Time series of 91-day running mean $PC_1^{*2} + PC_2^{*2}$, showing the low-frequency (primarily interannual) modulation of the variance of the MJO mode (blue) and the BSISO mode (red).

Fig. 14

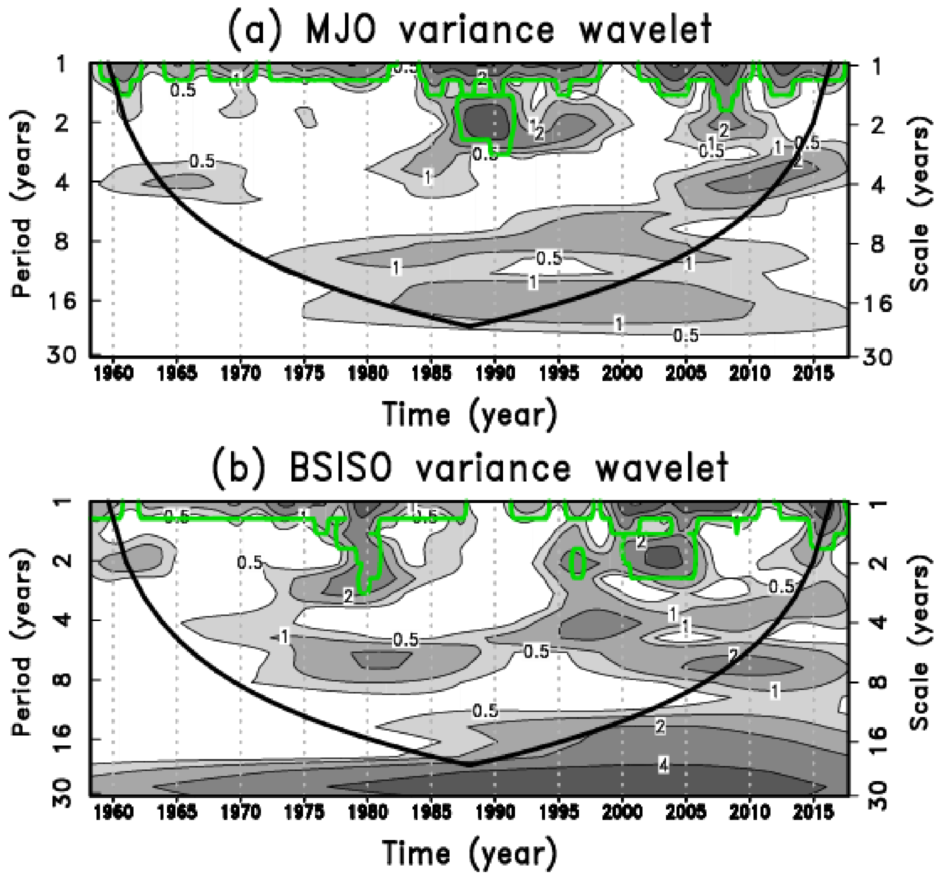

Fig. 15 The local wavelet power spectrum of the 3 month running mean (a) MJO and (b) BSISO amplitudes. The left axis is the Fourier period (in yr) corresponding to the wavelet scale on the right axis. The bottom axis is time (yr). The green contour encloses regions of greater than 90% confidence for a red-noise process with a lag-1 coefficient. The cone of influence is indicated by the thick curved lines.

Fig. 15

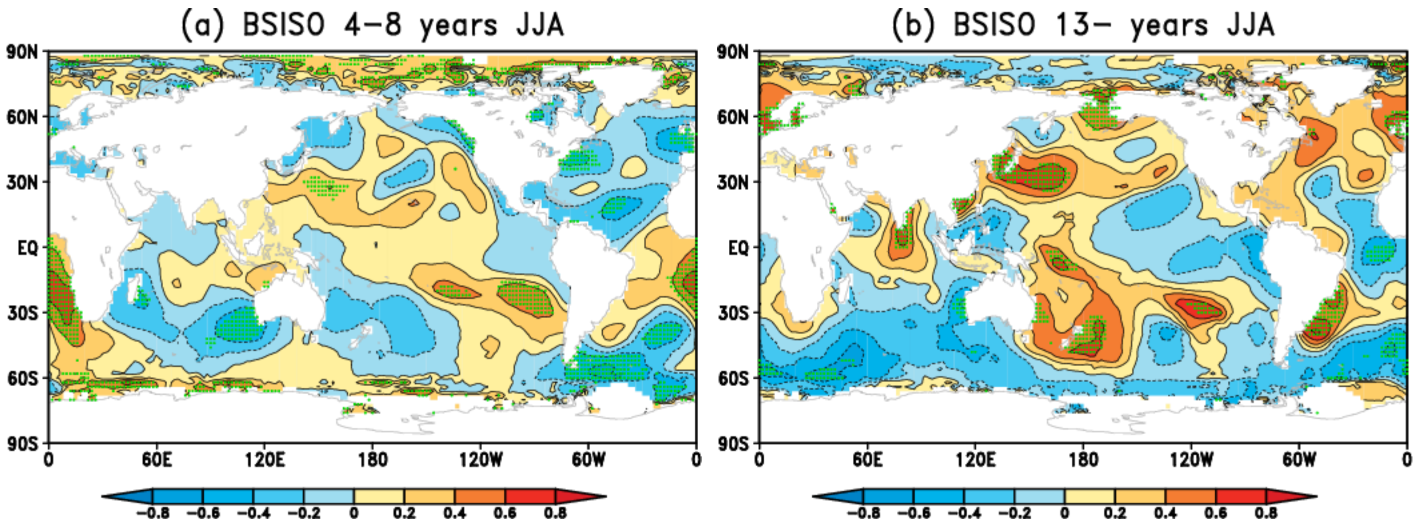

Fig. 15 Correlations between the BSISO activity and SST anomalies during JJA on (a) interannual (4-8 years) and (b) interdecadal (longer than 13 years) timescales. Anomalies on the interannual and interdecadal timescales are isolated, after removing the linear trend, by retaining the 8-16th and 1-5th components of the Fourier transform, respectively. The green marks represent where the correlations are significant at the 90% confidence level.

Fig. 16

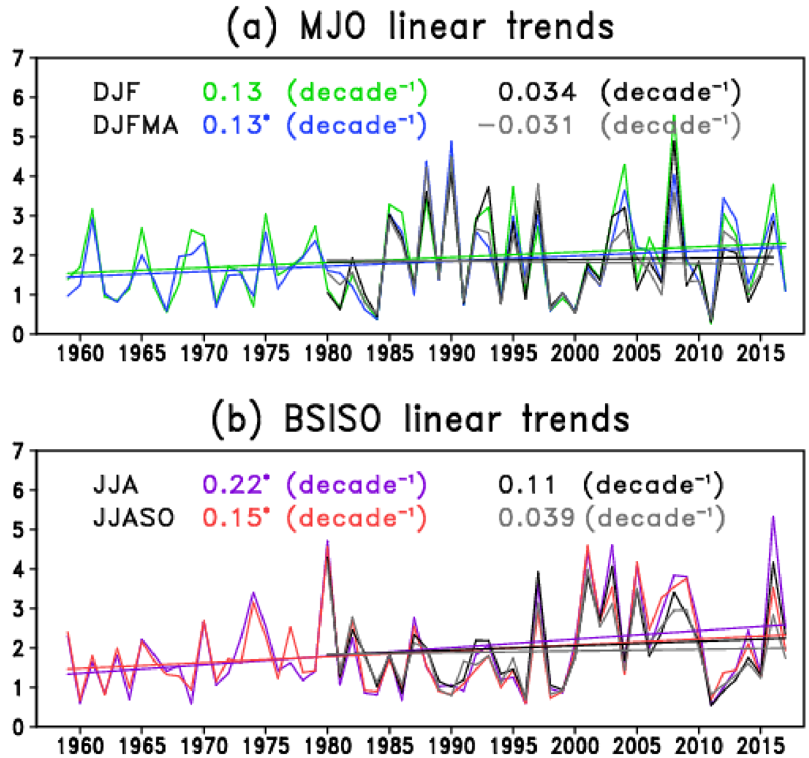

Fig. 16 Time series of the (a) MJO and (b) BSISO modes in terms of $PC_1^2 + PC_2^2$ averaged over the specified months indicated. The values are linear trend (decade^{-1}) and those with asterisk denote 90% significance.